Polystyrene Particles Reveal Pore Substructure As They Translocate

Matthew Pevarnik,[†] Ken Healy,[†,‡,*] Maria Eugenia Toimil-Molares,[§] Alan Morrison,[‡] Sonia E. Létant,[⊥] and Zuzanna S. Siwy[†,*]

[†]Department of Physics and Astronomy, University of California, Irvine, Irvine, California 92697, United States, [‡]Department of Electrical and Electronic Engineering, University College Cork, Cork, Ireland, [§]Department of Materials Science, GSI Helmholtzzentrum für Schwerionenforschung GmbH, Darmstadt, Germany, and [⊥]Physical and Life Sciences Directorate, Lawrence Livermore National Laboratory, Livermore, California 94550, United States

ABSTRACT

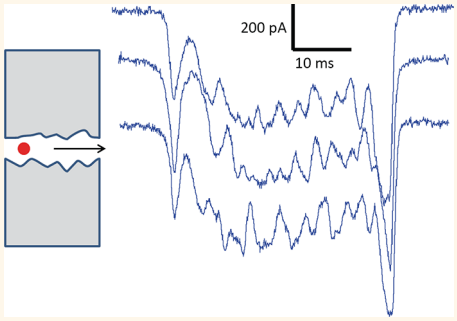

In this article, we report resistive-pulse sensing experiments with cylindrical track-etched PET pores, which reveal that the diameters of these pores fluctuate along their length. The resistive pulses generated by polymer spheres passing through these pores have a repeatable pattern of large variations corresponding to these diameter changes. We show that this pattern of variations enables the unambiguous resolution of multiple particles simultaneously in the pore, that it can detect transient sticking of particles within the pore, and that it can confirm whether any individual particle completely translocates the pore. We demonstrate that nonionic surfactant has a significant impact on particle velocity, with the velocity decreasing by an order of magnitude for a similar increase in surfactant concentration. We also show that these pores can differentiate by particle size and charge, and we explore the influence of electrophoresis, electroosmosis, and pore size on particle motion. These results have practical importance for increasing the speed of resistive-pulse sensing, optimizing the detection of specific analytes, and identifying particle shapes.

KEYWORDS: nanopore · nanoparticle · resistive-pulse technique · ion current

Resistive-pulse sensing involves the detection and analysis of particles as they pass through a channel or pore separating two reservoirs of electrolyte solution. The resistance of that pore is monitored by applying a voltage between the reservoirs, which drives a flux of ions through it, detected as a current flowing from the voltage source. Particles may be driven through the pore electrokinetically, by pressure, or simply move by diffusion, and they modulate the flux of ions as they pass through, thus inducing pulses in the measured resistance. In addition to counting particles, analysis of these pulses allows estimation of particle size,[1,2] electrophoretic mobility,[3] effective charge,[4] and measurement of the size and volume of the pore used to analyze those particles.[3]

The first example of resistive-pulse sensing was the Coulter counter,[1] developed to count and size blood cells. The Coulter counter has since been used to characterize a variety of analytes, including bacteria,[5] mitochondria,[6] and gas bubbles.[7] With the advent of track-etched pores,[8] resistive-pulse sensing was extended to counting and sizing nanoscale particles, such as polystyrene spheres[9] and viruses.[3,10] Later, ion channels enabled sensing of polymers[11−13] and small molecules,[14−21] as well as of nucleic acids[22] and proteins,[23] and are now on the cusp of sequencing DNA.[24−26] Recently, resistive-pulse sensing has been demonstrated with solid-state nanopores,[27−29] silica nanochannels,[30] gold nanoconstriction,[31] and PDMS nanochannels.[32]

It was noted in the past[3,7,9] that electrical fluctuations within a resistive pulse correspond to physical variations in the structure of the nanopore. However, this has seen little application, used only to determine the base and tip diameters of a conical pore[3] and to reveal the tapered shape of glass nanopipettes.[33−35] In addition, although surfactant is routinely added to the particle solution to prevent aggregation and mitigate pore clogging, the significant impact of surfactant on particle velocity has never been reported.

In this article, we report on the resistive-pulse sensing of polystyrene spheres passing through track-etched polyethyleneterephthalate (PET) pores. Our results show that the diameter of these pores fluctuates repeatedly along their length, which we

* Address correspondence to kenh@eleceng.ucc.ie; zsiwy@uci.edu.

Received for review May 31, 2012 and accepted July 15, 2012.

Published online July 15, 2012
10.1021/nn302413u

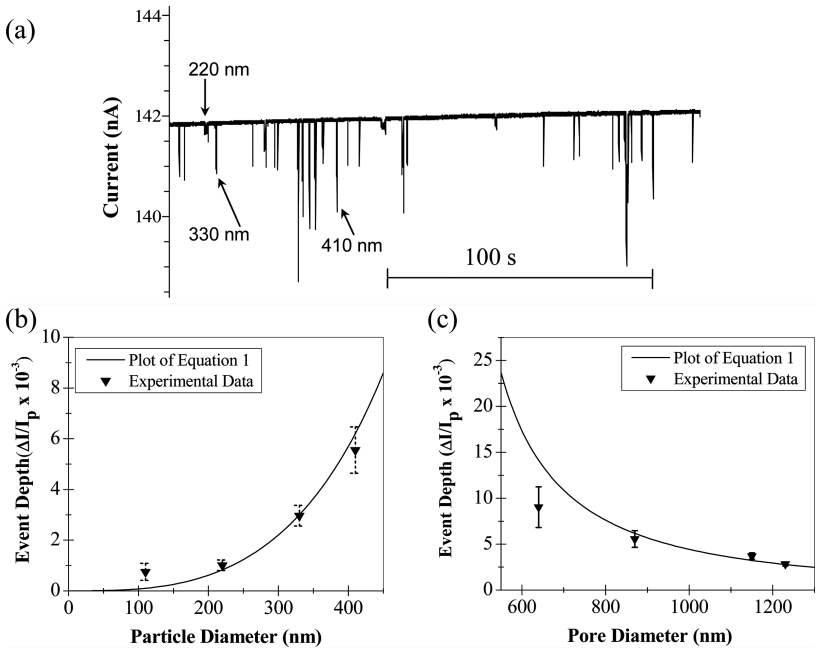

Figure 1. (a) Ionic current *vs* time for an 870 nm diameter pore at 300 mV with 220, 330, and 410 nm particles in 1 M KCl, pH 8, with 0.1% Tween 80. The concentration of each particle size was ~2 × 10^9 particles/mL. Each transient drop in current corresponds to a single particle passing through the pore; example translocations of 220, 330, and 410 nm particles are indicated. Note that the slow variation in the baseline was simply a consequence of variations in laboratory temperature occurring on the minutes time scale. The magnitude of this slow variation was ~1% of the baseline current throughout the whole measurement. (b, c) Agreement of our data with eq 1 for event depth *vs* particle diameter for an 870 nm pore (b) and event depth *vs* pore diameter for 330 nm particles (c). Note that this equation is not fit to our data; it does not have any free parameters; $I_{particle} = I_p$.

analyze by studying the corresponding variations in the measured resistive pulses. We demonstrate that this repeatable pattern of variations in the ion current signal allows unambiguous resolution of multiple particles in the pore at once and detection of particles transiently sticking in the pore. Compared to classical Coulter counter systems, resistive-pulse sensing using pores with varying cross-section can thus be performed at higher analyte concentrations, since multiple events can be easily resolved. We also believe that particles of the same size and charge, but different shapes, will modulate these resistive-pulse signals in distinct ways due to the varying pore cross-section, thus allowing differentiation between them.

To the best of our knowledge, the resistive-pulse technique is the only nondestructive method of studying the internal structure of high aspect ratio pores. It has been shown recently that the structure of the pore walls can significantly influence ionic transport through nanopores,[36] and for many applications of nanoporous membranes, *i.e.*, capacitors, drug-delivery systems, separations, it is important to quantify the pore geometry and wall structure. The method we have presented to predict the internal pore structure from the ion current signal during particle translocation is also applicable to other nanopore and nanofluidic systems. Finally, we show that a 20-fold increase in surfactant concentration leads to an approximately 20-fold decrease in particle velocity, which is potentially of practical importance for optimizing the detection of specific analytes.

RESULTS AND DISCUSSION

Particle Translocations Reveal Internal Pore Structure. Carboxyl-functionalized polystyrene particles with diameters of 220, 330, and 410 nm suspended in 1 M KCl solution were electrophoretically driven through an approximately cylindrical 870 nm diameter track-etched pore in a PET membrane, resulting in a transient drop, or "event", in the ionic current as each particle passes through. Figure 1a shows the ionic current on a long time scale, where it can be seen that the event depths are clustered around specific levels. It has been shown in the past that the depth is a function of particle volume and pore geometry,[3,9,30,37,38] and for particles whose size is comparable to the pore diameter the event depth follows the relation[9,30]

$$\frac{R_{particle} - R_{empty}}{R_{empty}} = \frac{D}{L}\left[\frac{\sin^{-1}\left(\frac{d}{D}\right)}{\sqrt{1-\left(\frac{d}{D}\right)^2}} - \frac{d}{D}\right] = \frac{I_{empty} - I_{particle}}{I_{particle}} \quad (1)$$

as shown in Figure 1b, c. Here, d is the particle diameter, D is the pore diameter, L is the pore length,

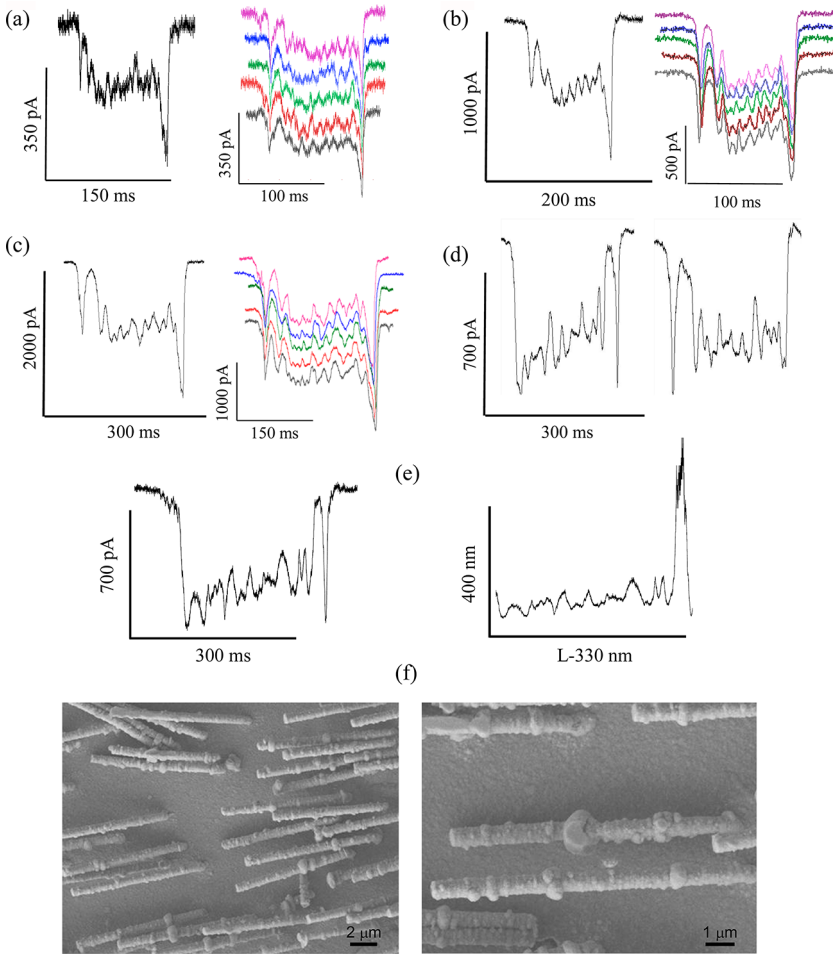

Figure 2. (a–c) Magnified views of the ionic current events from Figure 1a for 220, 330, and 410 nm particles, respectively, showing that the events have a characteristic pattern of variations irrespective of particle size. A single event is shown on the left, while the right shows 5 events, vertically offset from each other to facilitate comparison. In order to highlight the reproducibility of this characteristic pattern of variations, Figure S2 shows 20 events superimposed on one another. The events are linearly stretched in the *x*-direction so that the beginning and end of each are aligned, to compensate for slight variations in the mean particle velocity. (d) Events for 330 nm particles passing in opposite directions through a different pore, 520 nm mean diameter, showing that the pattern of variations is reversed for the opposite particle direction. (e) An example of a single 330 nm nanoparticle passing through the same 520 nm in diameter pore together with the pore diameter profile according to the formula given in ref 9 (eq 2). Note that this plot may not be accurate in the *x*-direction, as the particle velocity cannot be assumed constant. L is the pore length. (f) SEM images of gold replicas of similar PET pores. Gold was electrodeposited into the pores, and then the PET membrane dissolved so that the interior of the pores could be imaged. This process necessitated using membranes containing 10^7 pores/cm^2 to acquire suitable images in a reasonable time. These membranes were etched under the same conditions as the single-pore membranes used for particle translocations.

$R_{particle}$ and R_{empty} are the electrical resistance with and without a particle, and $I_{particle}$ and I_{empty} are the equivalent currents. The pore diameter D was estimated from conductivity measurements assuming cylindrical pore geometry. The value $I_{particle}$ was calculated as an average current blockage in time within each event with respect to the baseline current in the vicinity of that event. Fitting the data shown in Figure 1b using a different approach that relates the event depth with minimum pore diameter as found from the maximum blockage within each event gave similar results (see Supporting Information).

Magnified views of individual events (Figure 2a–c left side) show large variations in current, and these variations occur in a specific pattern that is maintained for all events. This is highlighted on the right side of Figure 2a–c, which presents several events vertically offset to facilitate comparison. DeBlois and Bean observed similar, albeit smaller, fluctuations[9] and proposed that they were due to variations in the pore diameter along its length. We set out to prove this. We found that the pattern of fluctuations is maintained for different particle sizes (Figure 2a–c for 220, 330, and 410 nm particles, respectively). In addition, passing the particles in opposite directions through a pore (Figure 2d), an approach used before when translocating particles through glass pipettes,[33–35] shows that the pattern of fluctuations is reversed. Note that the left event shows an increasing trend apart from the final dip, which was observed only for particles passing in

this direction. We do not yet have an explanation for this.

As would be expected, the pattern of fluctuations is unique to a particular pore, as can be seen by comparing Figure 2a–c with Figure 2d.

For a specific nanopore, the structure of ion current events observed with particles of different sizes is very similar (Figure 2a–c, Figure S2). However, the ion current modulations are more pronounced for larger particles, since they obstruct more of the ions flowing through the pore. Although smaller particles can probe the pore with higher spatial resolution (similar to tips in atomic force microscopy), the reduced signal-to-noise ratio creates a trade-off. We note, however, that the particle size does not set a limit on the spatial resolution, as improved results can be achieved by deconvolution. The ultimate limits are the measurement bandwidth, noise, and the deviations in the particle shape from a perfect sphere. In our future studies we will investigate a wider range of particle sizes and determine the optimal particle size *vs* pore diameter that gives the highest spatial resolution. In addition, we will statistically study the duration and amplitude of the subpeaks within the ion current events. This analysis will allow us to map the velocity variations as a particle passes through the pore and relate these to local variations in the electric field in the pore.

Finally, SEM images of metal replicas of pores etched under the same conditions show significant variations in diameter along the pore length (Figure 2f), which confirms our hypothesis that the current modulations reflect the varying pore diameter along its axis. In PET pores etched under somewhat different conditions, diameter variations have been attributed to the laminar nature of the film, such that the etchant can penetrate deeper at the interfaces between the strata.[39] We estimated the variations in pore diameter using the first component in the equation derived by DeBlois *et al.*[9] (eq 2), and an example of this is plotted in Figure 2e. Note that this is only accurate in the radial direction, as the particle velocity is unlikely to be constant as it moves through the pore.

$$\Delta R = \frac{8\rho d^3}{3\pi D^4}\left[1+\frac{4}{5}\left(\frac{d}{D}\right)^2+\frac{24}{35}\left(\frac{d}{D}\right)^4+\ldots\right] \quad (2)$$

ρ in eq 2 indicates solution resistivity.

Characteristic Ionic Current Variations Shed Light on Particle Motion. This characteristic pattern of ionic current variations as each particle translocates reveals details about particle motion within the pore. Resolving multiple particles within the pore at the same time, a traditional problem for Coulter counting, becomes straightforward because the instances of the pattern corresponding to each particle can easily be recognized, as shown in Figure 3a. This is of practical importance, since higher analyte concentrations can be used to provide faster results. Currently, the concentration must be set low enough that multiple-particle events are statistically improbable. In addition, it is possible to clearly identify when particles get stuck within the pore, which is indicated by a pause in the characteristic pattern (Figures 3b, S3). The duration and position of this pause reveal how long the particle is stuck and the point where that happens. For example, the current event shown in the right panel of Figure 3b indicates that the particle got stuck in the beginning of the translocation process. Finally, the characteristic pattern allows us to determine if particles always completely translocate through the pore, rather than, for example, enter, partially translocate, and exit back out on the same side. In our experiments, particles always translocated completely through the pore. In addition, as highlighted by Sun and Crooks,[40] if individual particles enter and exit the pore multiple times, the occurrence of translocation events in time would not follow a Poissonian distribution. As expected, our data are Poissonian (not shown).

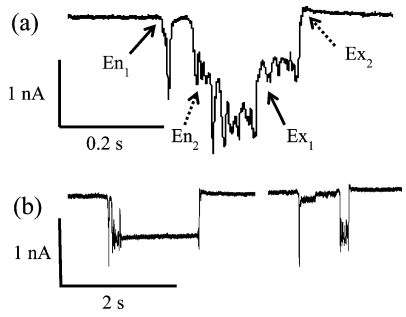

Figure 3. (a) Two particles passing through a pore simultaneously. Note that the ionic current variations enable the motion of each particle to be resolved independently. Solid and dashed arrows indicate the entry (En) and exit (Ex) of each particle. (b) Examples of particles temporarily sticking in the nanopore. The time and location at which they become immobilized are evident from the interruption of the characteristic pattern of ionic current variations (details of the event on the left are shown in Figure S3). For (a) and (b), the particles were 330 nm in diameter in 1 M KCl, pH 8, with 0.1% Tween 80. The same 520 nm mean diameter pore as in Figure 2d was used, and the applied voltage was 300 mV.

Size and Charge Discrimination. As has been done in the past, for example in refs 4, 9, 30, and 31, we demonstrate discrimination between particles of different sizes. Figure 4a shows a scatter plot of event depth *vs* duration for a mixture of 330 and 410 nm particles passing through an 870 nm pore. It is evident that the events are clustered according to their size, so that they can be discriminated in a mixture. As discussed earlier, the particle volume can be computed from the event depth and pore geometry. Figure 4a also highlights that events differ, not only in depth, but also in duration. Ito *et al.* have shown that event duration depends on the effective charge of the particle, in tandem with hydrodynamic drag.[4] Following their work, we explored charge sensitivity by studying a

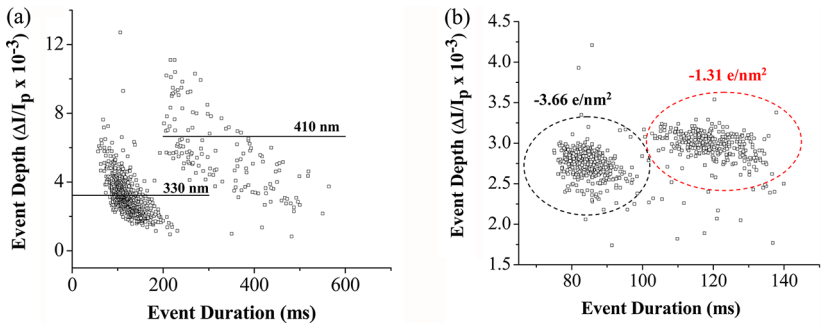

Figure 4. (a) Scatter plot of event depth *vs* duration for a mixture of 330 and 410 nm particles. Note that events for each particle size are clustered together and easily distinguishable. The particles were analyzed with an 870 nm mean diameter pore, in a solution of 1 M KCl, pH 8, with 0.1% Tween 80. The applied voltage was 300 mV. The concentration of each particle size was ~2 × 10^9 particles/mL. The straight lines indicate event depth as calculated from eq 1. (b) Scatter plot for a mixture of two types of 410 nm particles with fully ionized surface charge densities of −1.31 and −3.66 *e*/nm^2. Again, the events fall into two distinct clusters, differing significantly in event duration, corresponding to the two different particle types. More charged particles translocate the pore faster than less charged particles. The particles were suspended in 100 mM KCl, pH 8, with 0.1% Tween 80. The applied voltage was 150 mV. The pore used in this experiment had a mean diameter of 1360 nm.

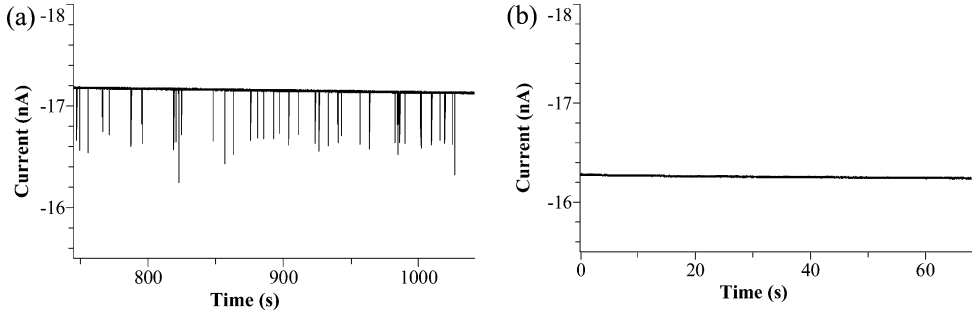

Figure 5. (a) Transport of 400 nm uncharged PMMA particles through a 700 nm mean diameter pore by electroosmotic flow. The experiment was carried out at pH 10 to ensure the pore surface charges were fully ionized.[41] The applied voltage was −500 mV, which means that the particles moved in the opposite direction of that which would be expected for electrophoretic transport of negatively charged particles. The particles were suspended in 100 mM KCl with 0.1% Tween 80. (b) Control experiment performed at pH 3 with otherwise identical conditions, showing that no particle translocations are observed when the electroosmotic flow is eliminated by protonating the surface charges.

mixture of 410 nm carboxyl-functionalized polystyrene particles, differing only in surface charge. Figure 4b plots event depth *vs* duration for this experiment and shows that the particle types can be clearly distinguished based on event duration, even though there is negligible difference in event depth (the sizes calculated from the mean depths are within the distribution of sizes measured using a Zetasizer, Nano ZS, Malvern Instruments, Ltd.).

Note that we cannot apply the method of Ito *et al.*[4] to calculate particle charge, as they assume a system free of electroosmosis, consistent with their uncharged carbon nanotube pores. Our pores have a negative surface charge, and we do not currently have the ability to apply pressure in our experimental setup so that we can measure that charge to account for electroosmosis.

Electroosmosis. Track-etched PET pores are known to have −COOH surface groups that are negatively charged at basic pH,[41] which is likely to induce electroosmotic flow, as demonstrated recently in other nanopore systems.[42,43] To confirm this, we carried out experiments with uncharged poly(methyl methacrylate) (PMMA) particles, which should not experience electrophoresis. At pH 3, when the surface groups are fully protonated, and thus there should be no electroosmotic flow, we do not observe any particle translocations (Figure 5b). However, at pH 10, when the surface groups should be completely ionized, particles are observed translocating through the pore toward the cathode, which is the direction of electroosmotic flow (Figure 5a). The lack of translocations observed in the electrophoretic direction (positive voltages) confirms that the PMMA particles used in the experiments were indeed uncharged, indicating that no significant hydrolysis of the ester bonds occurred at pH 10. Thus, in our experiments with negatively charged particles, electroosmosis opposes particle transport, reducing the velocity compared to electrophoresis alone. The tests for electroosmosis were performed in 0.1 M KCl rather than 1 M KCl to enhance the effect of surface charges on ionic and particle transport.

Translocation Velocity As a Function of Pore Diameter. Figure 6a plots the velocity of 330 nm particles through pores of a range of sizes. It can be seen that the velocity increases by over an order of magnitude as the mean

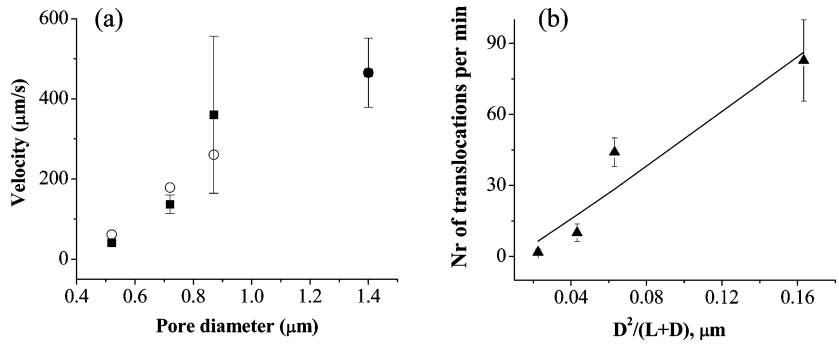

Figure 6. (a) Mean particle velocity (squares) as a function of pore size, compared to velocities calculated from the reduction factors presented by Paine and Scherr[44] (circles) with respect to the velocity for the largest pore (mean diameter 1400 nm). Particles were suspended in 1 M KCl, 40 mM Tris, pH 8, with 0.1% Tween 80. (b) Number of translocations of 330 nm particles per minute through pores of different diameters, presented as a function $D^2/(L + D)$, where D and L are pore diameter and length, respectively.[45] The applied voltage was 300 mV.

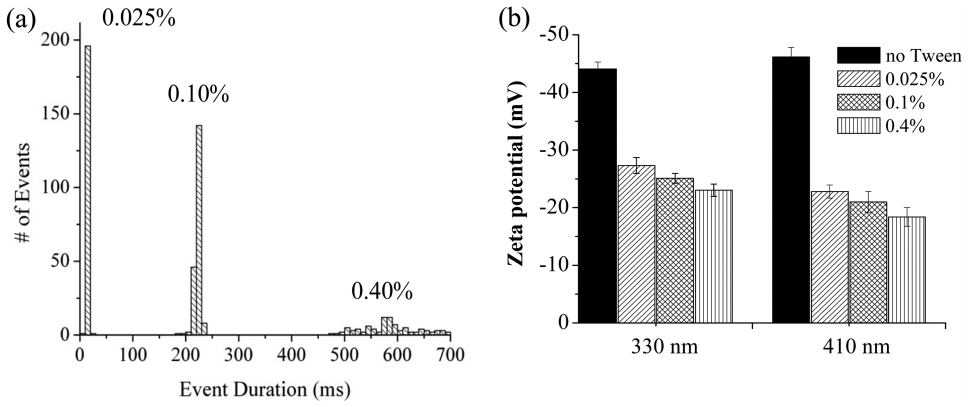

Figure 7. (a) Influence of Tween 80 surfactant concentration on the velocity of 410 nm particles passing through a 1360 nm mean diameter pore. The applied voltage was 300 mV. (b) Zeta potentials for 330 and 410 nm particles measured in a range of surfactant concentrations show that the effective charge decreases with increasing surfactant concentration. For both (a) and (b), the particles were suspended in 100 mM KCl, pH 8, with the % (v/v) Tween 80 indicated in the figure.

pore diameter increases from 520 to 1400 nm. In a narrow pore, the proximity of the walls will introduce hydrodynamic drag, slowing particle translocation.[44] We find that the corresponding velocity reduction factors computed by Paine and Scherr[44] with respect to the velocity in a 1400 nm in diameter pore accurately describe our data (Figure 6a). In the calculations, only electrophoretic transport was considered. Also, as expected with smaller pores, due to the decreased volume in which particles can be captured by the electric field, the event rate also decreases with pore size (Figure 6b). According to the modeling proposed by Nakane *et al.*,[45] the rate of collisions of particles with the pore opening scales with the pore diameter as $D^2/(L + D)$ if the applied voltage assures that each nanoparticle arriving at the pore mouth will translocate the pore. Our data are indeed in agreement with the model (Figure 6b).

Influence of Surfactant. Although surfactant is routinely added in resistive-pulse sensing, to avoid particles sticking to each other or the pore, the effect of that surfactant on particle motion has been little explored. Crooks *et al.* noted that uncharged particles behave as if they have an effective positive charge when using the nonionic surfactant Triton X-100.[40] With the same surfactant, they also observed that the effective charge of carboxyl-modified polystyrene particles was significantly lower than the number of ionizable −COOH functional groups.[4] We show that the event duration, and thus mean particle velocity, depends very significantly on the concentration of surfactant (in our case Tween 80). Figure 7a shows that for an approximately 20-fold increase in Tween 80 concentration the particle velocity decreases by a similar factor. Note that changes in the solution viscosity are not responsible, as it remains the same (data not shown). Our reasoning for this correlation follows the hypothesis proposed by Sun and Crooks.[40] that crown-ether-like interactions between K^+ ions and particle-bound Tween 80 molecules bind K^+ ions to the particle, making its effective charge more positive. To support this hypothesis, we measured the zeta potential of these particles in various surfactant concentrations (Figure 7b). For a fixed particle size and electrolyte concentration, surface charge is proportional to zeta potential,[46] which indicates that the effective particle charge does

decrease with increasing surfactant concentration. Note that the instrument used was not capable of measuring zeta potential with the 1 M KCl concentration used in many of our resistive-pulse sensing experiments, due to its high conductivity.

As would be expected, since the particles have more time to diffuse at lower velocity, the distributions of translocation times are broader for higher surfactant concentration.

CONCLUSIONS

We have demonstrated resistive-pulse sensing in long cylindrical pores with undulating diameters. As particles pass through these pores, they consistently generate resistive pulses with a repeatable electrical pattern mapping the physical variations of the pore's structure. This pattern gives several advantages and unique capabilities compared to typical resistive-pulse sensing. It can detect transient sticking of particles in the pore, it can confirm whether any individual particle completely translocates the pore, and it allows unambiguous detection of multiple particles in the pore, which would previously corrupt the results, so that higher analyte concentrations can be used for faster analysis. In addition, these resistive-pulse variations due to the pore structure have the potential to enable differentiation between particles of the same volume and charge, but with different shapes. We have found that the concentration of surfactant used has a significant effect on the particle translocation velocity. This has not been previously reported and is potentially useful for optimizing the sensor for different analytes. We have also shown the differentiation of particles based on size and charge and confirmed that both electrophoresis and electroosmosis are significant driving forces for particle translocation. Our results also highlight that as the pore diameter approaches the particle size, hydrodynamic drag due to the pore wall slows the particles. Future work will focus on detailed statistical analysis of the peaks and troughs present in each translocation event, which carry information on local variations in the particle velocity as well as the pore structure. In addition, the translocation of particles of different shapes will be studied.

MATERIALS AND METHODS

Track-Etched Pores. All experiments presented in this article were performed with single polymer pores prepared by the track-etching technique.[8,47] The technique involved irradiation of 12 μm thick polyethylene terephthalate foils with single energetic heavy ions (*e.g.*, 11.4 MeV/u Au and U ions) at the UNILAC linear accelerator of the GSI Helmholtzzentrum für Schwerionenforschung, Darmstadt, Germany, and subsequent chemical etching in 0.5 M NaOH at 70 °C. Under these etching conditions, the pores are generally cylindrical. The mean pore diameter scales linearly with the etching time, with 0.5 h of etching resulting in approximately 100 nm diameter pores. The mean pore diameter can be estimated more precisely by measuring the pore conductance in a solution of known conductivity, based on the membrane thickness and the assumption of a cylindrical geometry.

Polystyrene Particles. The particles used in these experiments were purchased from Bangs Laboratories (Fisher, IN, USA), and all specifications quoted below were reported by the manufacturer. The carboxyl-functionalized (PS−COOH) particles used had nominal diameters of 120, 220, 330, and 410 nm, with corresponding surface charge densities of −0.53, −1.10, −3.75, and −3.66 e/nm^2. Particles of 410 nm diameter with a surface charge density of −1.31 e/nm^2 were also used in the experiment presented in Figure 4b only. In addition, 400 nm unfunctionalized poly(methyl methacrylate) particles were used to explore electroosmotic transport. All particles were suspended in solutions of 0.01, 0.1, and 1 M KCl, with 0.1% v/v Tween 80 unless otherwise noted. For pH 8 and 10, the solutions were buffered with 0.4 mM Tris and adjusted to the desired pH with HCl or NaOH unless otherwise noted; for pH 3, the pH was adjusted with HCl. Particle concentrations were in the range 10^8 to 10^{10} particles/mL. Particle sizes and zeta potentials were measured with a Zetasizer Nano ZS (Malvern Instruments, Westborough, MA).

Experimental Setup. A PET membrane with a single pore was mounted between the chambers of a custom-made conductivity cell. Particle solution was placed in one chamber only, and solution without particles was placed in the other. Ag/AgCl electrodes (chloridated Ag wire) were used to apply voltage and measure ionic current. The current was measured with an Axopatch 200B amplifier (Molecular Devices, Sunnyvale, CA, USA), filtered at 1 kHz using the Axopatch filter, and digitized at 10 kHz with a Digidata 1322A (Molecular Devices). Voltages were applied to the chamber without particles, and the other side was connected to a ground, such that a positive voltage would electrophoretically draw negatively charged particles through the pore. The conductivity cell and Axopatch headstage were placed inside a faraday cage (Warner Instruments, Hamden, CT, USA) on a vibration isolation table (TMC, Peabody, MA, USA), to minimize noise. Data were analyzed using a custom MATLAB (Mathworks, Natick, MA, USA) code.

Preparation of Metal Replica of Pores. Membranes containing 10^7 pores/cm^2 were obtained by chemical etching of 12 μm thick PET foils subjected to heavy ion irradiation with 10^7 ions/cm^2 (UNILAC linear accelerator at the GSI Helmholtzzentrum für Schwerionenforschung, Darmstadt, Germany). The chemical etching was performed for 3 h in 0.5 M NaOH, 70 °C. Gold nanowires were electrodeposited using a gold sulfite-based bath, at 50 °C, applying −0.7 V. Under these conditions, the gold adopts the shape of the hosting channel. After dissolution of the PET membrane in 9 M NaOH, SEM images of the Au wires reveal the inner morphology of the hosting pores.

Conflict of Interest: The authors declare no competing financial interest.

Supporting Information Available: Comparison of experimentally measured event depth with an alternative model to the one shown in the main text is presented. Superposition of ion current events from Figure 1a and details of the event in Figure 3b are shown as well. This material is available free of charge *via* the Internet at http://pubs.acs.org.

Acknowledgment. Irradiation with swift heavy ions was performed at the GSI Helmholtzzentrum für Schwerionenforschung GmbH, Darmstadt, Germany. This research was supported by the National Science Foundation (CHE 0747237) and UC National Lab Fee Program (09-LR-09-116432-SIWZ). This work was performed under the auspices of the U.S. Department of Energy by Lawrence Livermore National Laboratory under Contract DE-AC52-07NA27344. K. H. acknowledges the financial support of the European Union FP7 Marie Curie Program (PIOF-GA-2008-220492). We are grateful to Gael Nguyen and Florian Haurais for their support in imaging the metal replicas of the pores.

REFERENCES AND NOTES

1. Coulter, W. H. Means for Counting Particles Suspended in a Fluid. U.S. Pat. No. 2,656,508, 1953.
2. Coulter, W. H. High Speed Automatic Blood Cell Counter and Cell Size Analyzer. *Proc. Natl. Electron. Conf.* **1956**, *12*, 1034–1042.
3. DeBlois, R. W.; Bean, C. P.; Wesley, R. K. A. Electrokinetic Measurements with Submicron Particles and Pores by the Resistive Pulse Technique. *J. Colloid Interface Sci.* **1977**, *61*, 323–335.
4. Ito, T.; Sun, L.; Crooks, R. M. Simultaneous Determination of the Size and Surface Charge of Individual Nanoparticles Using a Carbon Nanotube-Based Coulter Counter. *Anal. Chem.* **2003**, *75*, 2399–2406.
5. Kubitschek, H. E. Electronic Counting and Sizing of Bacteria. *Nature* **1958**, *182*, 234–235.
6. Gear, A. R. L.; Bednarek, J. M. Direct Counting and Sizing of Mitochondria in Solution. *J. Cell Biol.* **1972**, *54*, 326–345.
7. Berge, L. I.; Feder, J.; Jøssang, T. A Novel Method to Study Single-Particle Dynamics with Resistive Pulse Technique. *Rev. Sci. Instrum.* **1989**, *60*, 2756–2763.
8. Fleischer, R. L.; Price, P. B.; Walker, R. M. *Nuclear Tracks in Solids: Principles and Applications*; University of California Press: Berkeley, CA, 1975.
9. DeBlois, R. W.; Bean, C. P. Counting and Sizing of Submicron Particles by the Resistive Pulse Technique. *Rev. Sci. Instrum.* **1970**, *41*, 909–916.
10. DeBlois, R. W.; Wesley, R. K. A. Sizes and Concentrations of Several Type C Oncornaviruses and Bacteriophage T2 by the Resistive-Pulse Technique. *J. Virol.* **1977**, *23*, 227–233.
11. Bezrukov, S. M.; Vodyanoy, I.; Parsegian, V. A. Counting Polymers Moving through a Single Ion Channel. *Nature* **1994**, *370*, 279–281.
12. Krasilnikov, O. V.; Rodrigues, C. G.; Bezrukov., S. M. Single Polymer Molecules in a Protein Nanopore in a Limit of a Strong Polymer-Pore Attraction. *Phys. Rev. Lett.* **2006**, *97*, 018301 (1−4).
13. Oukhaled, A. G.; Biance, A.-L.; Pelta, J.; Auvray, L.; Bacri, L. Transport of Long Neutral Polymers in the Semidilute Regime through a Protein Nanopore. *Phys. Rev. Lett.* **2012**, *108*, 088104 (1−4).
14. Bezrukov, S. M. Ion Channels as Molecular Coulter Counters to Probe Metabolite Transport. *J. Membr. Biol.* **2000**, *174*, 1–13.
15. Movileanu, L. Squeezing a Single Polypeptide through a Nanopore. *Soft Matter* **2008**, *4*, 925–931.
16. Howorka, S.; Siwy, Z. S. Nanopore Analytics: Sensing of Single Molecules. *Chem. Soc. Rev.* **2009**, *38*, 2360–2384.
17. Robertson, J. W. F.; Rodrigues, C. G.; Stanford, V. M.; Rubinson, K. A.; Krasilnikov, O. V.; Kasianowicz, J. J. Single-Molecule Mass Spectrometry in Solution Using a Solitary Nanopore. *Proc. Natl. Acad. Sci. U. S. A.* **2007**, *104*, 8207–8211.
18. Kukwikila, M.; Howorka, S. Electrically Sensing Protease Activity with Nanopores. *J. Phys.: Condens. Matter* **2010**, *22*, 454103 (1−6).
19. Borsenberger, V.; Mitchell, N.; Howorka, S. Chemically Labeled Nucleotides and Oligonucleotides Encode DNA for Sensing with Nanopores. *J. Am. Chem. Soc.* **2009**, *131*, 7530–7531.
20. Mitchell, N.; Howorka, S. Chemical Tags Facilitate the Detection of Individual DNA Strands with Nanopore. *Angew. Chem., Int. Ed.* **2008**, *47*, 5565–5568.
21. Astier, Y.; Kainov, D. E.; Bayley, H.; Tuma, R.; Howorka, S. Stochastic Detection of Motor Protein-RNA Complexes by Single-Channel Current Recording. *Chem. Phys. Chem.* **2007**, *8*, 2189–2194.
22. Kasianowicz, J. J.; Brandin, E.; Branton, D.; Deamer, D. W. Characterization of Individual Polynucleotide Molecules Using a Membrane Channel. *Proc. Natl. Acad. Sci. U. S. A.* **1996**, *93*, 13770–13773.
23. Movileanu, L.; Howorka, S.; Braha, O.; Bayley, H. Detecting Protein Analytes That Modulate Transmembrane Movement of a Polymer Chain within a Single Protein Pore. *Nat. Biotechnol.* **2000**, *18*, 1091–1095.
24. Venkatesan, B. M.; Bashir, R. Nanopore Sensors for Nucleic Acid Analysis. *Nat. Nanotechnol.* **2011**, *6*, 616–624.
25. Cherf, G. M.; Lieberman, K. R.; Rashid, H.; Lam, C. E.; Karplus, K.; Akeson, M. Automated Forward and Reverse Ratcheting of DNA in a Nanopore at 5-Å Precision. *Nat. Biotechnol.* **2012**, *30*, 344–348.
26. Manrao, E. A.; Derrington, I. M.; Laszlo, A. H.; Langford, K. W.; Hopper, M. K.; Gillgren, N.; Pavlenok, M.; Niederweis, M.; Gundlach, J. H. Reading DNA at Single-Nucleotide Resolution with a Mutant MspA Nanopore and Phi29 DNA Polymerase. *Nat. Biotechnol.* **2012**, *30*, 349–353.
27. Li, J.; Stein, D.; McMullan, C.; Branton, D.; Aziz, M. J.; Golovchenko, J. A. Ion-Beam Sculpting at Nanometre Length Scales. *Nature* **2001**, *412*, 166–169.
28. Harms, Z. D.; Mogensen, K. B.; Nunes, P. S.; Zhou, K.; Hildebrand, B. W.; Mitra, I.; Tan, Z.; Zlotnick, A.; Kutter, J. P.; Jacobson, S. C. Nanofluidic Devices with Two Pores in Series for Resistive-Pulse Sensing of Single Virus Capsids. *Anal. Chem.* **2011**, *83*, 9573–9578.
29. Tsutsui, M.; Hongo, S.; He, Y.; Taniguchi, M.; Gemma, N.; Kawai, T. Single-Nanoparticle Detection Using a Low-Aspect-Ratio Pore. *ACS Nano* **2012**, *6*, 3499–3505.
30. Saleh, O. A.; Sohn, L. L. Quantitative Sensing of Nanoscale Colloids Using a Microchip Coulter Counter. *Rev. Sci. Instrum.* **2001**, *72*, 4449–4451.
31. Fraikin, J.-C.; Teesalu, T.; McKenney, C. M.; Ruoslahti, E.; Cleland, A. N. A High-Throughput Label Free Nanoparticle Analyzer. *Nat. Nanotechnol.* **2011**, *6*, 308–313.
32. Saleh, O. A.; Sohn, L. L. An Artificial Nanopore for Molecular Sensing. *Nano Lett.* **2003**, *3*, 37–38.
33. Lan, W. J.; Holden, D. A.; Zhang, B.; White, H. S. Nanoparticle Transport in Conical-Shaped Nanopores. *Anal. Chem.* **2011**, *83*, 3840–3847.
34. Lan, W. J.; Holden, D. A.; Liu, J.; White, H. S. Pressure-Driven Nanoparticle Transport across Glass Membranes Containing a Conical-Shaped Nanopore. *J. Phys. Chem. C* **2011**, *115*, 18445–18452.
35. Lan, W. J.; White, H. S. Diffusional Motion of a Particle Translocating through a Nanopore. *ACS Nano* **2012**, *6*, 1757–1765.
36. Cruz-Chu, E. R.; Ritz, T.; Siwy, Z. S.; Schulten, K. Molecular Control of Ionic Conduction in Polymer Nanopores. *Faraday Discuss.* **2009**, *143*, 47–62.
37. Kubitschek, H. E. Electronic Measurement of Particle Size. *Res. Appl. Ind.* **1960**, *13*, 128–135.
38. Gregg, E. C.; Steidley, K. D. Electrical Counting and Sizing of Mammalian Cells in Suspension. *Biophys. J.* **1965**, *5*, 393–405.
39. Mukaibo, H.; Horne, L. P.; Park, D.; Martin, C. R. Controlling the Length of Conical Pores Etched in Ion-Tracked Poly(ethylene terephthalate) Membranes. *Small* **2009**, *5*, 2474–2479.
40. Sun, L.; Crooks, R. M. Single Carbon Nanotube Membranes: A Well-Defined Model for Studying Mass Transport through Nanoporous Materials. *J. Am. Chem. Soc.* **2000**, *122*, 12340–12345.
41. Wolf, A.; Reber, N.; Apel, P. Yu.; Fischer, B. E.; Spohr, R. Electrolyte Transport in Charged Single Ion Track Capillaries. *Nucl. Instrum. Methods Phys. Res., Sect. B* **1995**, *105*, 291–293.
42. Firnkes, M.; Pedone, D.; Knezevic, J.; Döblinger, M.; Rant, U. Electrically Facilitated Translocations of Proteins through Silicon Nitride Nanopores: Conjoint and Competitive Action of Diffusion, Electrophoresis and Electroosmosis. *Nano Lett.* **2010**, *10*, 2162–2167.
43. Van Dorp, S.; Keyser, U. F.; Dekker, N. H.; Dekker, C.; Lemay, S. G. Origin of the Electrophoretic Force on DNA in Solid-State Nanopores. *Nat. Phys.* **2009**, *5*, 347–351.
44. Paine, P. L.; Scherr, P. Drag Coefficients for the Movement of Rigid Spheres through Liquid-Filled Cylindrical Pores. *Biophys. J.* **1975**, *15*, 1087–1091.
45. Nakane, J.; Akeson, M.; Marziali, A. Evaluation of Nanopores as Candidates for Electronic Analyte Detection. *Electrophoresis* **2002**, *23*, 2592–2601.
46. Hunter, R. J. *Zeta Potential in Colloids Science*; Academic Press: New York, 1981.
47. Spohr, R. *Methods and Device to Generate a Predetermined Number of Ion Tracks*. German Patent DE2951376 C2, Sept 15, 1983; U.S. Patent 4369370, 1983.